^{133}Xe(Cs) Mössbauer measurements on Ar, Ne, Kr, Xe, Rb, and Cs inclusions in W and Mo

K. Milants, P. Hendrickx, J. Verheyden, T. Barancira, W. Deweerd, and H. Pattyn
Instituut voor Kern-en Stralingsfysica, University of Leuven, Celestijnenlaan 200 D, B-3001 Leuven, Belgium

S. Bukshpan
Soreq Nuclear Research Center, Yavne, Israel

F. Vermeiren and G. Van Tendeloo
EMAT, Rijksuniversitair Centrum te Antwerpen, University of Antwerpen, Groenenborgerlaan 171, B-2020 Antwerpen, Belgium
(Received 3 September 1996; revised manuscript received 25 September 1996)

We report on an extended series of Mössbauer measurements on noble-gas (Ar, Ne, Kr, and Xe) and alkali (Rb and Cs) inclusions in Mo and W. Using TEM on some samples allowed a direct size distribution measurement. The sites occupied by the ^{133}Xe(Cs) probe atoms differ for small atomic rare-gas (Ne and Ar), large atomic rare-gas (Kr and Xe), and alkali inclusions. We followed the site population and inclusion sizes as a function of annealing temperature, observing the expected growth of the inclusions upon annealing due to distinct growth mechanisms. Temperature-dependent measurements show that two kinds of inclusions are formed: soft ones with a characteristic temperature which is too low to make them contribute to the Mössbauer spectrum and tough ones which are perfectly embedded in the matrix. Kr and Xe inclusions of the latter kind feature a characteristic temperature which (i) is remarkably independent of preparation conditions and (ii) greatly exceeds the largest possible value for pure rare-gas solids. We argue that this kind of solid rare-gas inclusion ''borrows'' its dynamical properties from the high Debye temperature matrix. [S0163-1829(97)01305-2]

I. INTRODUCTION

Due to the complete insolubility of rare gas or alkali impurities in most metals, their forced introduction, for instance, by ion implantation, up to a high dose will result in their precipitation as a second phase (Refs. 1 and 2). The precipitates are present in the form of solid phase fcc (rare gas)/bcc (alkali) inclusions in the bcc host matrix selected here, Mo and W. These inclusions are nanosized, often under high pressure and topotaxially aligned to the host matrix. A frequently observed axial alignment is the ⟨111⟩ direction of an fcc rare gas inclusion being oriented along the ⟨110⟩ direction of a bcc host material (Ref. 3). To reduce its interfacial energy, the inclusion often forms a (100)-truncated (111)-edged octahedron. See Fig. 1 for a schematic drawing of the ⟨100⟩ and ⟨111⟩ projection of this three-dimensional figure.

Transmission electron microscopy (TEM) observation allows one to obtain an overview image of the precipitation within the matrix. Figure 2 shows a plan view of Kr inclusions in an Al (fcc) foil. The local atomic concentration is 8 at. % and the sample has been annealed up to 400 °C for half an hour under Ar atmosphere. One can easily identify the truncated octahedral shape of the inclusions. The ⟨100⟩ direction of Kr is along the ⟨100⟩ direction of the Al matrix.

Figure 3 shows a plan view TEM picture of as-implanted

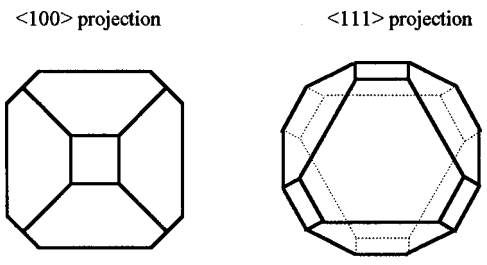

FIG. 1. Schematic drawing of the ⟨100⟩ and ⟨111⟩ projection of a truncated octahedron.

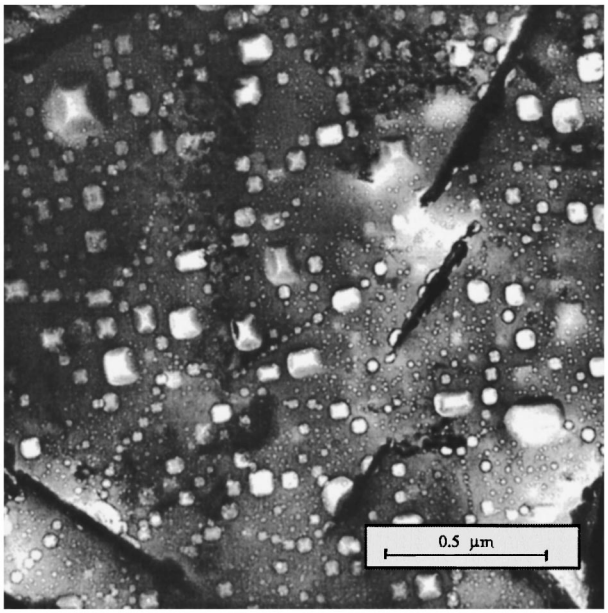

FIG. 2. Plan view TEM picture of 8 at. % Kr in Al annealed at 400 °C. The enlargement is 80 000.

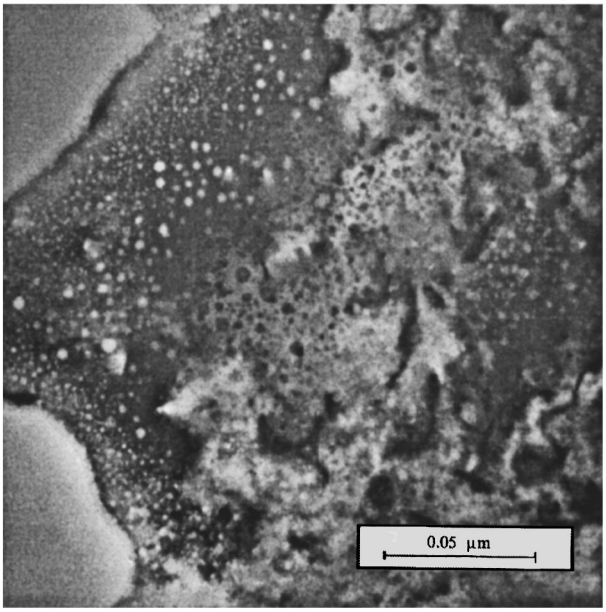

FIG. 3. Plan view TEM picture of 10 at. % Ne in Mo as implanted. The enlargement is 750 000.

Ne inclusions in polycrystalline Mo. The implantation dose of 2×10^{16} ions/cm^2 and energy of 16 keV correspond to a maximum local atomic concentration of 10 at. % at 120 Å beneath the sample surface. Since these inclusions are smaller than the Kr inclusions in Al, it is more difficult to distinguish them, but also in this case, we can recognize their truncated octahedral shape.

^{133}Xe(Cs) Mössbauer spectroscopy is a powerful technique to study the electronic and dynamical properties of Cs compounds, inclusions and impurities in materials (Ref. 4). In our case we use the technique for the study of rare gas and alkali metal inclusions in Mo and W.

The 81 keV Mössbauer transition in ^{133}Cs can be populated according to the decay scheme presented in Fig. 4. In the present case we use the decay of the ^{133m}Xe. Despite the relatively short half-life of this isotope high activity sources can be obtained from commercially available fission products.

All systems under study in this work were Mössbauer sources, produced by implantation of the radioactive Xe into the metallic matrices. Mössbauer resonances were obtained in transmission mode versus a single line absorber of CsCl.

The relatively small resonance linewidth of ^{133}Cs ($2\Gamma_0=2\times0.28$ mm/s) and the quadrupole moment of the excited state ($Q^*=-0.22$ b) allow quite sensitive measurements of the hyperfine interactions experienced by the Cs atom in a variety of electronic environments. The quadrupole moment of the ground state is too small to induce a visible splitting. The high energy of the Mössbauer transition results in a very low resonant fraction and requires low temperature measurements. On the other hand, this makes the resonance extremely sensitive to the dynamical parameters of the crystalline lattice surrounding the probe atom.

Mössbauer probe atoms implanted together with precipitating impurity atoms can reside on various lattice sites. Each of these positions gives rise to a different component in the Mössbauer spectrum. We expect contributions from essentially three major lattice sites. Probe atoms can appear in solid solution in the host metal and thus be located at substitutional lattice sites. [Vacancy associated sites (Ref. 5) are improbable because of the scavenging action of precipitate formation on vacancies.] They can reside at the interface between the inclusion and the surrounding metal or they can be situated inside the bulk of the inclusions. We are able to distinguish between these different lattice sites and separately study their dynamical properties. This ability forms the most important benefit of Mössbauer spectroscopy on ^{133}Cs.

II. SAMPLE PREPARATION

Both the stable and radioactive implantations were done at the Leuven Isotope Separator. The substrates consisted of W and Mo polycrystalline foils and Mo ⟨110⟩ single crystals. Our experience with the implantation of radioactive probes in an inclusion-metal system favors the implantation of the probe ions before the ions that are to form the inclusions. This enables the radioactive probe atoms to participate actively in the precipitation process and fewer probe ions will reside at the, for this study, less important substitutional site in the host metal. The radioactive ions were implanted at room temperature, with a fluence of about 1×10^{14} ions/cm^2 and with an energy of 80 or 90 keV for every sample. For the implantation of the inclusion material we performed theoretical calculations based on the TRIM program (Ref. 6) taking into account sputtering. Three implantations with different energies are usually sufficient to obtain a nearly homogeneous implantation profile, encompassing the implanted probe atom distribution. We chose the implantation doses for every implantation in such a way that the mean local atomic concentration of the inclusion ions ranges from 1 to 10 at. %. An example of a theoretical profile calculation for a concentration of 2 at. % Kr in W is shown in Fig. 5. We obtain this profile for a simulated implantation of subsequently 4.5×10^{15} at./cm^2 at an energy of 125 keV, 1.5×10^{14} at./cm^2 at 50 keV, and 3×10^{14} at./cm^2 at 20 keV.

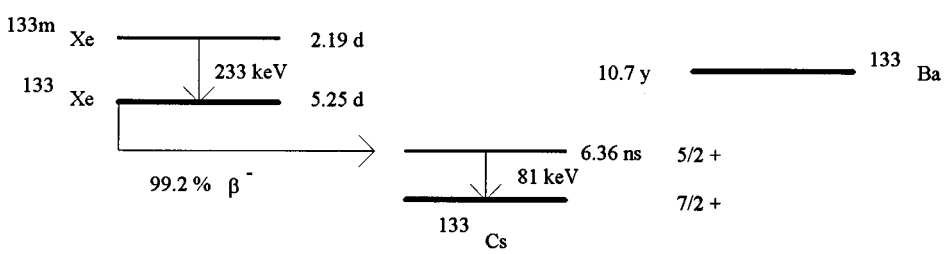

FIG. 4. The decay scheme of ^{133m}Xe/^{133}Xe.

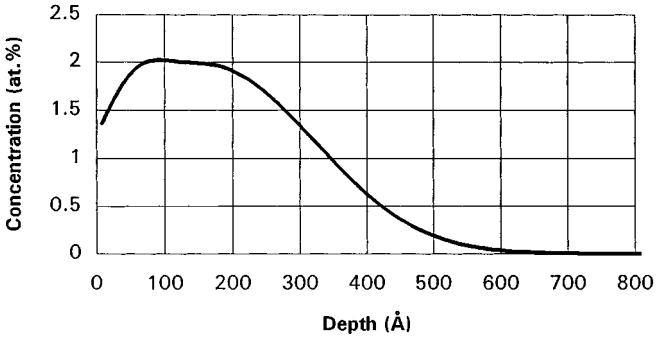

FIG. 5. Calculated implantation profile for 2 at. % Kr in W.

III. EXPERIMENT

We used an exchange gas cryostat to perform the Mössbauer measurements. The source, attached to a constant acceleration drive, was mounted inside the exchange gas tube. It could be kept at temperatures between 4.2 and 100 K. The CsCl absorber (300 mg Cs/cm^2, corresponding to an effective absorber thickness $t_{\text{absorber}} \approx 2$) was mounted inside the liquid helium container. Its temperature therefore was fixed at 4.2 K independent on any heating of the source.

We analyzed the spectra with the fitting program ''MOSAUT'' (Ref. 7). This program offers the possibility to fit a series of spectra consistently in a way that parameters can be fitted with the same value for all spectra in a series. Since the resonance lines are not resolved in our spectra, this option renders the fitting procedure much more reliable.

For the analysis of the spectra where source and absorber had a different temperature, the second order Doppler shift (Ref. 8) has been taken into account. For TEM observations a Philips CM20 instrument, operating at 200 kV, was used.

IV. RESULTS

First we recorded two reference spectra. We implanted a low dose of 5×10^{13} at./cm^2 ^{133}Xe in Mo and W. In both cases we fitted the spectrum with one single line and one quadrupole split component. The isomer shift of the single line with respect to CsCl was -1.28 mm/s for Mo and -1.60 mm/s for W. These isomer shifts correspond to probe atoms located at substitutional lattice sites. For the Mo sample, the contribution of this single line in the spectrum was larger than 80% and for the W sample it was larger than 60%. The presence of a quadrupole split component shows that part of the probe atoms, even after a low dose implantation, are situated at defect associated sites (Ref. 5).

After the implantation of the inclusion material, the spectra become more complex. We will discuss the rare gas and alkali metal postimplantations separately.

A. Postimplantation with large rare-gas ions (Kr and Xe)

The best fit for each series of Kr and Xe rare gas inclusions was obtained when we allowed three spectral components. An example of a fitted Xe series is given in Fig. 6. The site assignment for the three components is explained in the following discussion.

The first component is a single line with the same isomer shift as the substitutional component in the reference spectra.

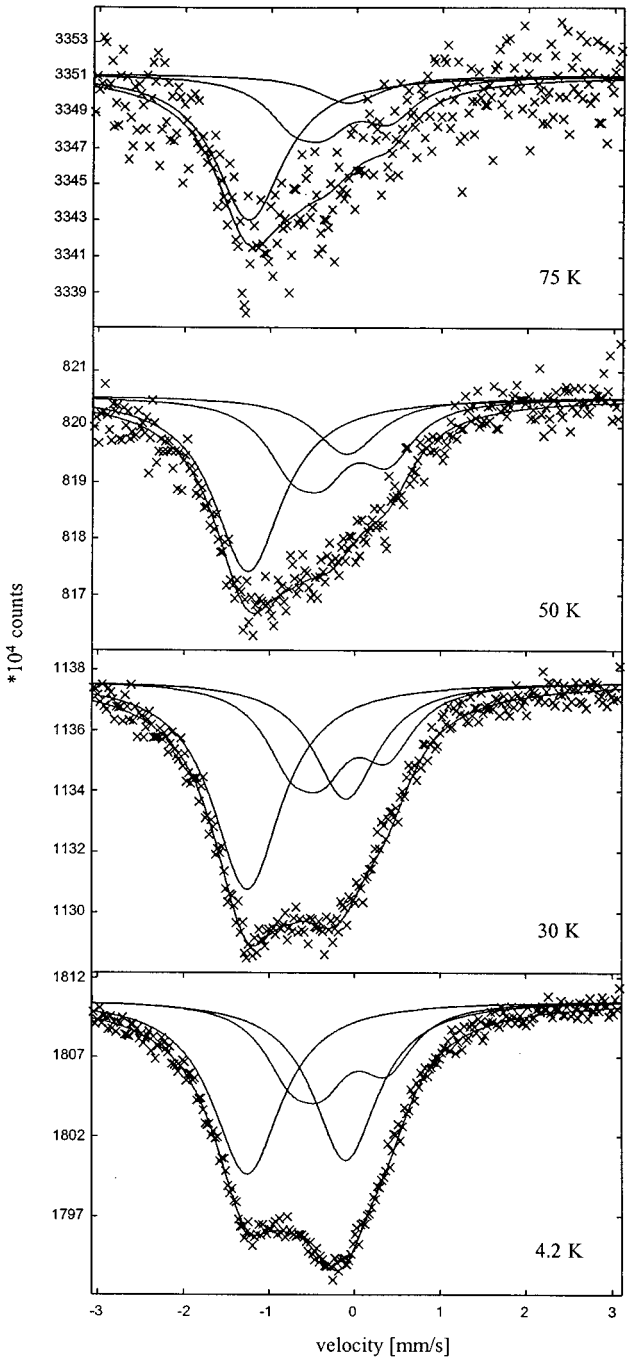

FIG. 6. Fitted series of ^{133}Cs Mössbauer spectra from Xe inclusions in Mo. The measuring temperatures are indicated.

It has a narrow linewidth (stemming from a well defined site) and its characteristic Mössbauer temperature θ_M is close to the known value of 262 K (Ref. 9) and an estimated 296 K for the substitutional site in Mo and W, respectively. It is straightforward to ascribe this component to probe atoms on a cubic symmetric substitutional lattice site in the metal host matrix. We will refer to this component as the substitutional component.

The second component is a single line with an isomer shift lying between the isomer shift of ^{133}Cs in Cs metal [-0.222 mm/s for $6s^{n=1.23}$ (Ref. 10)] and in $CsMnF_3$ [$+0.044$ mm/s for $6s^{n=0}$ (Ref. 11)]. The ^{133}Cs probes ap-

pear to be in a charge state between +1 and 0. This component is attributed to a matrix isolated cubic symmetric substitutional site inside the solid rare gas inclusions. The characteristic temperature is much lower than for the substitutional site. This component is referred to as the inclusion component.

The third component is a quadrupole split component with an isomer shift larger than the inclusion isomer shift but smaller than the substitutional isomer shift. Its characteristic temperature also lies between the values of the two other sites. We fitted this component with an asymmetry parameter η equal to zero, in view of our very limited sensitivity to its precise value. The value of the resulting quadrupole splitting yields a lattice electric field gradient V_{zz}(latt) of the order of 10^{16} V/cm^2. This is comparable to values that have been found for surface sites for NaW (Ref. 12) and CdCu (Ref. 13). Therefore we suggest that these probe atoms are situated at the inclusion-metal interface. This component is called the interfacial component.

Because the components are not resolved in the spectra, we fitted each series of spectra several times with different isomer shifts for the inclusion site. The χ^2 of the series is observed to have a minimum. This procedure again renders the resulting fit more reliable.

B. Postimplantation with alkali ions (Rb and Cs)

A slightly different situation is observed for the case of alkali inclusions. We will explain this for Cs inclusions (first presented in Ref. 14) where a fit of the spectra with the three components which we employed in the Kr and Xe case yielded unacceptable results. Isomer shift values of the inclusion component ranged from −0.29 to +0.20 mm/s, while that of Cs metal is −0.222 mm/s (Ref. 10), decreasing even further with compression. Excluding the component which we initially described as the inclusion site, makes the χ^2 of the fit only slightly worse. This leaves us two possibilities: (i) the Xe probe atoms segregate out of the alkali inclusions or (ii) the Xe probe atom remains inside the inclusions but does not contribute to the spectrum due to a very low characteristic temperature. Later on, we will show the former one to be more probable. We observed the same behavior for the Rb inclusions.

C. Postimplantation with small rare-gas ions (Ne and Ar)

Ne and Ar inclusions form a particular case. At first, we analyzed our Mössbauer spectra in a manner analogous to the heavier rare gases, allowing three spectral components (Ref. 15). The existence of an inclusion site is however doubtful for a number of reasons.

(1) There is a very large size difference between the Ne and Ar inclusion atoms and the Xe probe atoms [$R_{Ne}/R_{Xe}=0.71$, $R_{Ar}/R_{Xe}=0.87$ (Ref. 16)], probably driving the latter out of solution. The Hume-Rothery size rule, which we corroborated recently by Mössbauer measurements on rare gas mixtures of Ar in Xe (Ref. 17), indeed predicts 0.85 as a lower limiting ratio for a stable solution of large size atoms into small atom material.

(2) We kept the samples at room temperature during implantation and while transporting them to the cryostat. The Xe probe atoms thus had sufficient time to possibly segregate out of the Ne and Ar inclusions.

(3) The isomer shifts obtained from the three-site fit for the inclusion site in Ne and Ar have a value of about 0.25 mm/s, much larger than the limiting value of 0.044 mm/s measured for $CsMnF_3$ [$6s^{n=0}$ (Ref. 11)]. This would imply that the Cs probe carries a negative charge, which is improbable, even more so since one rather expects a positive charge state after the nuclear decay.

Therefore, we analyzed the same data, this time without inclusion component. This procedure makes the overall χ^2 only slightly worse.

We found nonetheless a strikingly good correspondence between inclusions sizes from TEM results and from the Mössbauer analysis *with* inclusion site on the Ne samples. We will comment on this later.

V. DISCUSSION

The results of the fits for all three inclusion types and the characteristic temperatures calculated from those are presented in Table I. The mean isomer shift of the substitutional component, taken over 120 spectra in Mo, yields a value of −1.27 mm/s with a standard deviation of 0.02 mm/s and −1.60 mm/s with a standard deviation of 0.03 mm/s over 45 spectra in W.

A. Quadrupole interaction at the interface

The quadrupole splitting of the interfacial component displays a puzzling behavior. It has a value of about −1.5 mm/s for the small rare gases, +2.5 mm/s for the large rare gases, and +1.8 mm/s for the alkali's in Mo. This corresponds to V_{zz} values of $+1.84\times10^{18}$ V/cm^2, -3.07×10^{18} V/cm^2, and -2.21×10^{18} V/cm^2, respectively. We interpret these by calculating V_{zz}(latt), using a simple point charge model, for an interfacial probe atom at a Mo (110) surface. Appendix A gives details. The best correspondence between the ratios of the measured and calculated values is found for probe distances above the Mo (110) surface of 0.5 Å for the small rare gases, 2.5 Å for the large rare gases and also for the Cs inclusion. A visual representation of the atomic configuration at the interface shows that this situation is quite possible, in view of the atomic sizes, since it corresponds to a probe atom which is situated quasisubstitutionally on a Mo lattice site in the case of small rare gas inclusions and essentially on an inclusion lattice site in the other cases.

This overall correspondence renders more confidence in the consistency of our interfacial site assignments as well as in the global spectral analysis, which we have conducted differently for Ne and Ar, Kr and Xe, Rb and Cs.

The corresponding calculated values for the quadrupolar asymmetry parameter η are 0.09 and 0.05 for the small and large rare gases and 0.03 for the alkali inclusions. This is close enough to zero, value which we used for fitting the Mössbauer spectra, not to influence the spectral shape.

B. Lattice dynamics of the inclusions

Temperature dependent Mössbauer measurements yield important information: we can deduce the fraction of probe

TABLE I. A survey of the measured values and the calculated characteristic temperatures with their standard deviation between brackets. N is the number of spectra in the series.

			Substitutional site			Interfacial site				Inclusion site		
	N	χ^2	IS mm/s	FWHM mm/s	θ_M K	IS mm/s	FWHM mm/s	QS mm/s	θ_M K	IS mm/s	FWHM mm/s	θ_M K
NeMo	37	275	−1.26	1.06	263 (35)	−0.10	1.05	−1.40	186 (14)			
ArMo	3	186	−1.29	1.1	252	−0.14	1.07	−1.52	162			
KrMo	28	277	−1.26	0.90	286 (27)	−0.28	0.95	2.26	247 (34)	−0.10	1.12	171 (29)
XeMo	9	250	−1.26	1.1	256 (22)	−0.24	0.79	2.52	217 (18)	−0.11	0.94	163 (22)
CsMo	33	380	−1.30	1.17	254 (26)	−0.37	1.18	1.88	204 (10)			
RbMo	10	287	−1.25	0.83	257 (12)	−0.34	1.03	1.81	214 (24)			
ArW	5	331	−1.65	1.07	277	−0.30	1.37	−2.08	229			
KrW	2	305	−1.69	1.00		−0.34	1.01	2.66		−0.09	0.82	
XeW	2	318	−1.65	1.16	272	−0.40	0.75	2.57	289	−0.18	1.58	188
CsW	28	287	−1.59	1.21	279 (30)	−0.37	1.24	2.00	208 (16)			
RbW	8	324	−1.56	0.91	257	−0.22	0.99	2.30	204			

ions contributing to each of the Mössbauer spectral components and extract lattice dynamics information for the corresponding site.

As we pointed out before, probe atoms in an inclusion system can be localized on various lattice sites, each of which has a different lattice dynamical coupling and therefore a different recoilless fraction. In this view, it is quite probable that some probe atoms end up in a site where they are so loosely bound that their contribution to the spectral intensity is negligible due to their extremely small f fraction in comparison to that of the other components. The chance of facing this state of affairs is quite large for our Mössbauer probe with its large transition energy of 81 keV. This would be the case, for instance, for a probe atom in uncompressed Xe and Cs, where it would have a chance of only 1/1640 and less than 1/100 000, respectively, to emit γ radiation without recoil. These probe atoms do nonetheless contribute to the baseline and thus dilute the total spectral intensity.

This fraction, a_0, forms what is commonly named the ''invisible'' fraction. It manifests itself as the remaining fractional population after the other ones which do contribute to the spectral intensity are accounted for: $a_0=1-\Sigma_k a_k$; $a_k=(\beta I_k/B)(1/f_k F_a)$. Here we have expressed a_k, the absolute fractional population of component k, in terms of its spectral intensity, I_k, a factor β, which accounts for any nonresonant spectral background, the baseline, B, its recoilless fraction, f_k, and a factor F_a, which is a function of the effective absorber thickness t_a: $F_a=(\Gamma_n\pi/2)t_a \exp(-t_a/2)[I_0(t_a/2)+I_1(t_a/2)]$ (Ref. 18). We calculate the recoilless fraction at the measuring temperature of the contributing component from its characteristic Mössbauer temperature, which we have first deduced from the temperature dependence of its spectral intensity.

From the original three components fit for Ne in Mo, we derived an invisible fraction of 42% (Ref. 15). From the relative intensity of the inclusion and interfacial component, we calculated a mean diameter of the inclusions contributing to the Mössbauer spectrum of 1.8(4) nm assuming the particles to be spherical. Analyzing the TEM micrograph from an identical sample (shown in Fig. 3) by means of a visually counting computer program, assuming spherical particles, yields the size distribution of the inclusions as shown in Fig. 7 (representing the volume percentage as a function of diameter). Surprisingly, this distribution is in nice accordance with the Mössbauer analysis based on a three-component fit: if 40% of the largest inclusions (where the pressure is lowest) would not contribute to the Mössbauer spectrum (corresponding to the invisible fraction), we would end up with a mean diameter of 2.3 nm of the remaining ones. This good correspondence makes us hesitate to state in a conclusive way that the Xe probes cannot be found inside the Ne inclusion in Mo system.

Extracting information about the dynamic properties of the inclusions is the main goal in performing temperature dependent measurements. The relative intensity of each component in the spectrum is proportional to the f fraction of that particular component. We then fit the dependency of the f fraction on temperature to a Debye model, and obtain a value for the Mössbauer characteristic temperature θ_M. This temperature is a measure for the bonding strength of the probe atom at its lattice position. If we want to relate this temperature to the Debye temperature of the probe's sur-

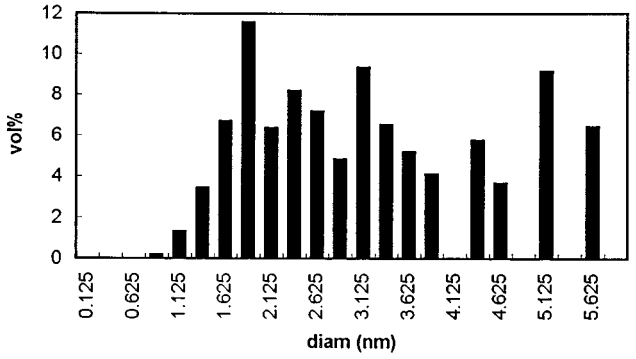

FIG. 7. Size distribution (given as volume percentage) of the Ne inclusions in Mo as obtained from Fig. 3 by an automatic counting program.

rounding lattice, we deal with an impurity problem. θ_M is equal to the Debye temperature θ_D of the probe's surrounding lattice only if the probe atom consists of the same element as its surrounding atoms (same mass and same binding force constants, as these properties influence the vibrational frequency and hence the characteristic temperature). For a ^{133}Xe(Cs) probe, this condition is approximately fulfilled for Xe or Cs inclusions. The general expression relating the two properties is (Ref. 19)

$$\left(\frac{\theta_M}{\theta_D}\right)^2 = \frac{A_{\text{impurity-host}}}{A_{\text{host-host}}} \frac{M_{\text{host}}}{M_{\text{impurity}}},$$

where A and M are the appropriate force constant and mass, respectively.

Table I gives an overview of the measured θ_M values in the rare gas and alkali inclusion systems under study. In Appendix B, we derive an estimation of the maximum θ_D value which can be achieved in bulk rare gases.

Our main observations are that (i) the θ_M values of Cs remain remarkably constant for each site, regardless of the inclusion or host material. This is also borne out by the small statistical fluctuation over the measuring series. (ii) The θ_M values in Kr and Xe are much higher than the maximal values which we can expect.

One explanation for the latter discrepancy could be the difference in θ_M and θ_D. If we want to correct for this in terms of the equation given before, we would have to accept that the force constant value between Cs and Xe is twice that between Xe and Xe. If we take the same approach for the Kr case, the ratio then would be 4.

Neither these large values nor their strong dependence on rare gas species are expected. We therefore suggest a different mechanism for the strong enhancement of θ_M.

We clearly observed rare gas inclusions of two kinds: in part of them the probe atom is loosely bound (very low θ_M) and in another part the probe atom is located on a site which exhibits an essentially constant and very high θ_M value, larger than the maximum for the bulk inclusion material. The first type of inclusions must be under very low pressure and have poor contact with the metal host lattice. In this case, the phonon spectrum is that of the solid rare gas and they form the invisible fraction, corresponding then to probe atoms located at the interface and inside these loosely bound inclusions. The second type of inclusions is exposed to a certain compression and the contact to the metal host lattice is very strong and intimate (as observed several times in high resolution TEM for topotaxially aligned inclusions). In this case the phonon spectrum is (partly) derived from and dictated by the hard metal matrix.

We find support for this view in electron diffraction work of Rossouw *et al.* on ArAl (Ref. 20). They found a mean θ_D of 142 K which also is far above the maximum value of 110 K for Ar.

A seemingly contradictory Mössbauer measurement was reported by Childress *et al.* (Ref. 21) on Fe-nanoparticles sputter deposited in Al_2O_3 and SiO_2. They observed a decrease of θ_D up to 40% with decreasing particle size, but this was accompanied by a concurrent increase of the relative lattice parameter a/a_0. In the case of noble gas inclusions on the contrary, it is known (Ref. 22) that a/a_0 decreases with decreasing particle size. Since the authors dealt with sputtered systems, we believe that in this case the interface registry may be much looser than in implanted systems.

Greuter *et al.* (Ref. 23) recently described Mössbauer experiments on KrAl, where they fitted a Mössbauer characteristic temperature for the inclusion site of 95(10) K. This value is equal to the maximal θ_D value for Kr inclusions. However, we found that we could fit their data very well with a combination of a 66% contribution from a strongly enhanced θ_D of 132 K together with a 34% contribution from $\theta_{\text{solid Kr}}$ of 56.5 K (which contributes to the Mössbauer spectral intensity because of the very low transition energy).

For the alkali inclusions, we tried to derive the minimum pressure a Cs inclusion should experience to warrant a measurable contribution of the ^{133}Cs probes inside this inclusion to the Mössbauer spectrum. We used the values from Refs. 24 for $\gamma(V)$ and $V/V_0(p)$. We found characteristic temperatures not exceeding 100 K for pressures up to 90 GPa. This means that the inclusion site in the case of Cs inclusions would essentially remain invisible for Mössbauer spectroscopy regardless of the inclusion pressure. We expect however that as in the case of the rare gases, the θ_M of the inclusion site would be strongly enhanced for at least part of the inclusions. The fact that we do not observe an inclusion site in these Mössbauer spectra, indicates that the Xe probe atoms have segregated out of the alkali inclusions.

C. Annealing behavior

Annealing of the implanted samples induces a global growth of the mean precipitate size. This behavior is known (Ref. 3) and we have also observed it by TEM on Kr inclusions in Al. The Mössbauer spectra on annealed samples reveal the expected behavior. Figure 8(a) shows the site occupation dependence on annealing temperature for Kr in Mo. The solid line connects the data points related to the visible inclusions (small size, good contact with Mo lattice). The dotted line connects the points related to the invisible fraction (large inclusions, poor contact with Mo lattice). The dashed line connects the points related to the substitutional occupation. Figure 8(b) displays the number of Kr atoms and the mean radius of the visible inclusions, calculated from the ratio of inclusion to interface occupation, assuming precipitates of spherical shape. From the combination of the two graphs, we can distinguish four temperature regions: 300–600 K, 600–700 K, 700–1000 K, and 1000–1100 K.

Vacancies in pure Mo become mobile at 425 K (Ref. 25). By trapping some of the vacancies created by the implantation, the inclusions are able to grow in the first temperature region and some of them become invisible because of two effects. (i) The pressure inside the growing inclusions decreases. (ii) Vacancies that are trapped at the interface of the inclusions may worsen the contact of the inclusion to the metallic host.

In the second region defect complexes at the interface of loosely bound inclusions dissociate. This results in a better contact of these inclusions to the host lattice, whereby some large invisible inclusions become visible, thereby increasing the mean radius of the visible inclusions. This mechanism of defect dissociation has also been observed in Ref. 26, where at temperatures of 570–670 K defect complexes of hydrogen, vacancies and neon dissociate from the interface of Ne

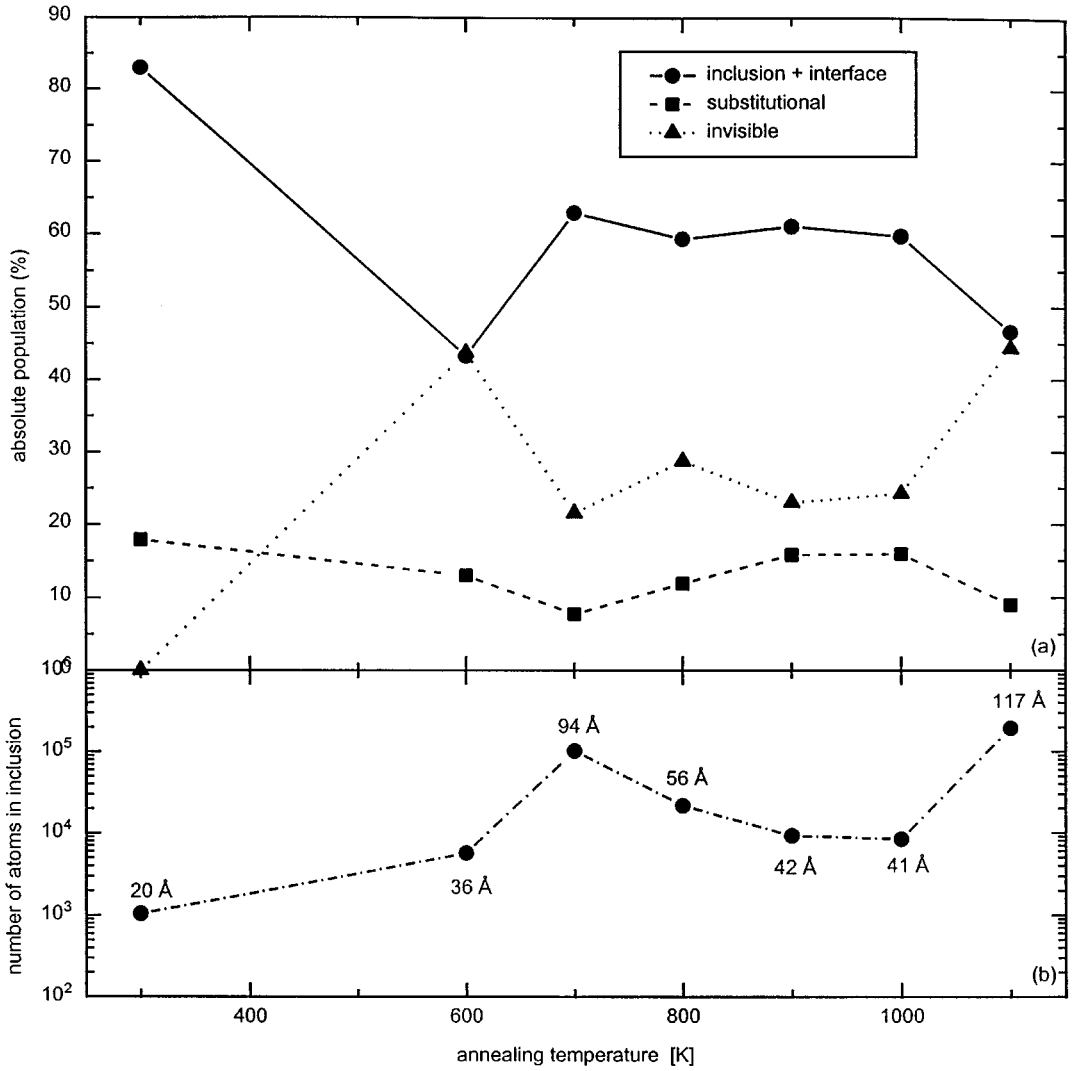

FIG. 8. Absolute site occupation of ^{133}Cs probes in a Mo sample containing Kr inclusions as function of annealing temperature.

precipitates in Mo. As stated in this article, the dissociation energy decreases slowly for larger inclusions.

The behavior in the third temperature region is puzzling at first sight. The ratio of the volume fractions of the visible and invisible inclusions remains constant, but the mean size of the visible inclusions decreases. There is also a slight increase of the substitutional fraction. We believe we observe the following mechanisms. As the invisible inclusions are under low pressure and have vacancies available at their surface, some of their outer gas atoms are able to leave the inclusion as an onset to Ostwald ripening. This process is responsible for the increase of the substitutional fraction. However, some of the material that left an invisible inclusion, precipitates in very small visible inclusions. This causes the mean radius of the visible inclusions to decrease. As surface diffusion is hampered by high pressure (Ref. 27), the mobility of these visible inclusions is strongly reduced. Together with the lack of supplementary vacancies, this causes the visible inclusions to remain small and under high pressure, even at high temperatures. Because the amount of transferred material from the invisible to the visible inclusions is so small, we do not see a change in the ratio of the occupied volume fractions.

In the last temperature region ($T \approx 0.5 T_m$), thermal vacancies arise in the Mo lattice. This is a bulk phenomenon and all inclusions can trap new vacancies. The result is, as in the first region, a global growth indicated by an increase of the mean precipitate size, a decrease of the substitutional fraction and an increase of the invisible fraction.

VI. CONCLUSION

Mössbauer spectroscopy is a very powerful technique to investigate rare gas and alkali inclusions in metals. We are able to distinguish between probe sites substitutional in the host metal, at the metal-inclusion interface and inside the inclusions. The behavior of these three sites as a function of annealing temperature reveals a global growth of the inclusion sizes. This conclusion is in general agreement with previous observations.

We have doubts about the occupation of an inclusion site in Ne, as we have arguments pro and contra the segregation of the probe ions out of the Ne inclusions. In the case of alkali precipitates, the Xe probe seems to have segregated.

Part of the probe atoms are situated at loosely bound lattice sites and do not contribute to the Mössbauer spectrum.

Some of the inclusions are therefore suggested to have a poor contact with the surrounding metallic host lattice. The probe atoms that do contribute to the Mössbauer spectra show a high Mössbauer characteristic temperature, compared to that of compressed bulk material. This observation brings us to the suggestion that the phonon spectrum of these inclusions is highly influenced by the surrounding metal matrix due to the intimate interfacial contact.

APPENDIX A

The relation between the total V_{zz} and V_{zz}(latt) originating from the charges surrounding the probe atom is (Ref. 28)

$$V_{zz}=V_{zz}(\text{latt})(1-\gamma_\infty)(1-K).$$

As we are only interested in the ratio of the calculated V_{zz}'s and in view of the uncertainties on the value of K, we keep the factor $(1-K)$ as a parameter.

Using $\gamma_\infty=-121$ for Cs (Ref. 29), we end up with

$$V_{zz}(\text{latt})=1.51\times10^{16}/(1-K)\ \ \text{V/cm}^2$$

for the small rare gases in Mo,

$$V_{zz}(\text{latt})=-2.52\times10^{16}/(1-K)\ \ \text{V/cm}^2$$

for the large rare gases in Mo,

$$V_{zz}(\text{latt})=-1.81\times10^{16}/(1-K)\ \ \text{V/cm}^2$$

for the alkalis in Mo.

To interpret these measured values, we calculated the V_{zz}(latt) for the interfacial site at a Mo (110) surface, using a point charge model. The orientation of the inclusion is such that its outer (111) planes are parallel to the (110) planes of Mo. In the point charge model, the electric field gradient tensor at the origin in the laboratory system (X,Y,Z) is given by the negative of a 3×3 matrix with components

$$V_{ij}=\sum_n q_n\,\frac{3i_nj_n-r_n^2\delta_{ij}}{r_n^5},$$

where i and j stand for X,Y,Z and n for the charged particles surrounding the probe atom, q is the charge of the particle, and r is the distance to the origin. Diagonalization of this tensor yields the description in the principal axis system (x,y,z). The resulting V_{xx}, V_{yy}, and V_{zz} define η $[=(V_{xx}-V_{yy})/V_{zz}]$ and V_{zz} with $|V_{zz}|\geqslant|V_{yy}|\geqslant|V_{xx}|$.

In the case of the rare gas inclusions, we consider only the Mo metal (110) surface as containing charged particles. We choose this charge to be equal to $+6$ for the Mo metal ions in accordance with the valence of Mo. For the Cs inclusions where both host and inclusion ions carry charges, we take for Mo $+6$ and for Cs $+1$. The only parameter responsible for the observed differences in the quadrupolar interaction is the distance of the interfacial probe atom to the Mo surface. We calculate V_{zz}(latt) for a probe atom as a function of its distance from a substitutional site in the Mo (110) surface.

APPENDIX B

Starting from the Grüneisen equation, we can derive an expression for the Debye temperature as a function of inclusion size. The Grüneisen parameter γ is defined in function of the Debye temperature θ and the volume of the unit cell V,

$$\gamma=-\frac{\partial\ \ln\theta}{\partial\ \ln V}$$

or

$$\theta(p)=\theta_0\exp\left[\gamma(V)\ \frac{V_0-V}{V_0}\right].$$

We will take the case of Xe inclusions as an example.

In order to calculate $\theta(p)$ as a function of size, we need to know V(size) and $\gamma(V)$. V(size) can be estimated from two equations: $V(p)$ from the equation of state (Ref. 30) and p(size) from the equation for the equilibrium bubble pressure which is a function of Γ, the interfacial tension, and r, the bubble radius (Ref. 3)

$$p_{\text{equilibrium}}=\frac{2\Gamma}{r}.$$

We recently deduced $\gamma(V)$ of isoelectronic CsI (Ref. 31). Taking this value for Xe and a value of 1.9 J/m^2 (Ref. 3) for Γ, a calculation of $\theta(p)$ as a function of the radius for Xe inclusions yields a maximum value of 107.6 K.

[1] C. Templier, C. Jouen, J. P. Rivière, J. Delafond, and J. Grilhé, C. R. Acad. Sci. Paris II **299**, 613 (1984).

[2] A. vom Felde, J. Fink, Th. Müller-Heinzerling, J. Pflüger, B. Scheerer, G. Linker, and D. Kaletta, Phys. Rev. Lett. **53**, 922 (1984).

[3] C. Templier, in *Fundamental Aspects of Inert Gases in Solids*, edited by S. E. Donnelly and J. H. Evans (Plenum, New York, 1991), p. 117.

[4] M. M. Abd-Elmeguid, Hyperfine Interact. **95**, 265 (1995).

[5] E. Verbiest and H. Pattyn, *Point Defects and Defect Interactions in Metals* (University of Tokyo Press, Tokyo, 1982), p. 485.

[6] J. F. Ziegler, J. P. Biersack, and U. Littmark, *The Stopping and Ranges of Ions in Solids* (Pergamon, New York, 1985).

[7] E. Verbiest, Comput. Phys. Commun. **29**, 131 (1983).

[8] W. L. Gettys and J. G. Stevens, in *Handbook of Spectroscopy*, edited by J. W. Robinson (CRC Press, Boca Raton, FL, 1981), Vol. 3, p. 505.

[9] E. Verbiest, Ph.D. thesis, University of Leuven, 1983.

[10] M. M. Abd-Elmeguid, H. Pattyn, and S. Bukshpan, Phys. Rev. Lett. **72**, 502 (1994).

[11] L. E. Campbell, in *Mossbauer Isomer Shifts*, edited by G. K. Shenoy and F. E. Wagner (North-Holland, Amsterdam, 1978), p. 781.

[12] R. F. Haglund, D. Fick, B. Horn, and E. Koch, Hyperfine Interact. **30**, 73 (1986).

[13] G. Schatz, R. Fink, T. Klas, G. Krausch, R. Platzer, J. Voigt, and

R. Wesche, Hyperfine Interact. **49**, 395 (1988).
[14] H. Pattyn, P. Hendrickx, K. Milants, J. De Wachter, and S. Bukshpan, Hyperfine Interact. **79**, 807 (1993).
[15] H. Pattyn, P. Hendrickx, and S. Bukshpan, in *Fundamental Aspects of Inert Gases in Solids*, edited by S. E. Donnelly and J. H. Evans (Plenum, New York, 1991), p. 243.
[16] A. Bondi, J. Phys. Chem. **68**, 441 (1964).
[17] S. Bukshpan, P. Hendrickx, K. Milants, and H. Pattyn, Phys. Rev. B **45**, 497 (1992).
[18] S. R. Reintsema, Ph.D. thesis, University of Groningen, 1976.
[19] B. Kolk, in *Dynamical Properties of Solids*, edited by G. K. Horton and A. A. Maradudin (Elsevier, Amsterdam, 1984), Vol. 5, p. 90.
[20] C. Rossouw and S. Donnelly, Phys. Rev. Lett. **27**, 2960 (1985).
[21] J. R. Childress, C. L. Chien, M. Y. Zhou, and Ping Sheng, Phys. Rev. B **44**, 11 689 (1991).
[22] R. C. Birtcher, in *Fundamental Aspects of Inert Gases in Solids*, edited by S. E. Donnelly and J. H. Evans (Plenum, New York, 1991), p. 133.
[23] M. Greuter and L. Niesen, J. Phys. Condens. Matter **5**, 3541 (1993).
[24] M. S. Anderson, E. J. Gutman, J. R. Packard, and C. A. Swenson, J. Phys. Chem. Solids **30**, 1587 (1969); D. B. McWhan, G. Parisot, and D. Bloch, J. Phys. F **4**, L69 (1974); R. Boehler and M. Ross, Phys. Rev. B **29**, 3673 (1984); D. Götzel and A. K. McMahan, *ibid*. **20**, 3210 (1979); K. Takemura, O. Shimomura, and H. Fujihisa, Phys. Rev. Lett. **66**, 2014 (1991).
[25] F. Lee, J. Matolich, and J. Moteff, Radiat. Eff. **60**, 53 (1982).
[26] J. Keinonen and V. Karttunen, Phys. Rev. B **37**, 8440 (1988).
[27] L. J. Perryman and P. J. Goodhew, Acta Metall. **36**, 2685 (1988).
[28] R. S. Raghavan, E. N. Kaufmann, and P. Raghavan, Phys. Rev. Lett. **34**, 1280 (1975); P. Raghavan, E. N. Kaufmann, R. S. Raghavan, E. J. Ansaldo, and R. A. Naumann, Phys. Rev. B **13**, 2835 (1976).
[29] F. D. Feiock and W. R. Johnson, Phys. Rev. **187**, 39 (1969).
[30] M. Kumari and N. Dass, J. Phys. Condens. Matter **2**, 7891 (1990).
[31] H. Pattyn, M. M. Abd-Elmeguid, S. Bukshpan, K. Milants, and J. Verheyden, Phys. Rev. B **51**, 10 357 (1995).